

A MICROMECHANICAL PARAMETRIC OSCILLATOR FOR FREQUENCY DIVISION AND PHASE NOISE REDUCTION

Tristan O. Rocheleau, Ruonan Liu, Jalal Naghsh Nilchi, Thura Lin Naing, and Clark T.-C. Nguyen
University of California, Berkeley, USA

ABSTRACT

A capacitive-gap transduced micromechanical resonator array has demonstrated a first on-chip MEMS-based frequency divider with 61-MHz output generated from a 121-MHz electrical drive through use of a parametric oscillation effect that provides not only the 6 dB reduction in close-to-carrier phase noise expected for a frequency divide-by-two function, but also a remarkable 23 dB reduction in far-from-carrier noise provided by filtering with an extremely high mechanical Q of 91,500. Unlike conventional frequency dividers (i.e., prescalers), the parametric oscillator dispenses with active devices and their associated noise, and operates with close to zero power consumption, limited in principle only by the power required to overcome MEMS resonator loss, estimated here at 100 nW. With an output voltage swing of 450 mVpp generated from only 445 mVpp of input swing on a differential version of this MEMS divider, cascaded chains of fully passive dividers are possible, as needed for use in real-world phase-locked loops and frequency synthesizers.

INTRODUCTION

Frequency dividers have become essential components in phase-locked loops (PLL) and frequency synthesizers used a myriad of applications, from instrumentation to wireless handsets. In a typical frequency synthesizer application, frequency dividers often limit the achievable phase noise performance and contribute a large or even majority portion of the total power consumption. Common digital dividers offer good noise performance, but at the cost of power far in excess of that permissible for mobile applications and with poor scaling as frequency is increased, with 135 mW power consumption typical for a low-noise divide-by-16 at 3 GHz [1].

To alleviate this, injection-locked oscillator dividers [2] that lock a free running oscillator to an input signal at a harmonic of the oscillation frequency have emerged as lower power options at high frequencies. With operating power below 100 μ W even at GHz frequencies [3], such dividers present a compelling alternative to traditional technologies, but come with performance limitations due to the active transistors used to sustain oscillation [4].

To overcome these limitations, this paper introduces a new frequency divider design using a parametric amplification effect in a capacitive-gap transduced MEMS device, such as that of Fig. 1, based on an array of wine-glass disk resonators [5], or Fig. 2, based on a stand-alone device operating in a differential mode. Each of these parametric oscillators works via modulation of a frequency-determining parameter of a resonator, in this case electrical stiffness [6], at twice the resonance frequency. This produces an effect analogous to a child on a swing, where swinging legs modulate frequency (or stiffness), providing gain and enhancement of in-phase resonant motion that with sufficient pump strength drives the resonator into self-sustained oscillation. While performing

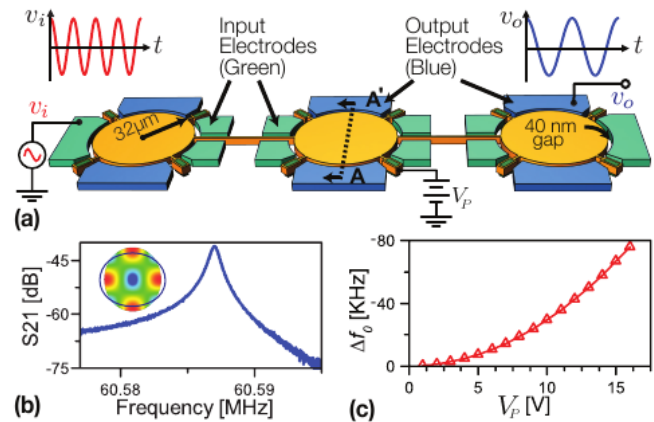


Fig. 1. Schematic view (a) of the wine-glass disk array parametric divider showing 121-MHz pump signal applied to the input electrodes (green) and resultant 60.6-MHz signal on the output electrodes (blue). (b) presents the high- Q frequency response of the resonator as measured by two-port transmission with a network analyzer, while (c) demonstrates the resonance frequency tuning required for parametric amplification through an electrical stiffness effect with applied voltage V_p

a frequency divide-by-two function, the single-ended version of Fig. 1 reduces phase noise by 6 dB at close-to-carrier frequencies and 23 dB far-from-carrier. Building upon this, the differential version of Fig. 2 enables an effective voltage gain, generating a measured output voltage swing of 450 mVpp, larger than the input swing of only 445 mVpp.

Though similar in operation to injection-locked frequency dividers, the parametric oscillator here requires no active devices, and thus, adds no additional noise sources beyond Brownian to the signal. Furthermore, with power consumption fundamentally limited only by the MEMS resonator loss, power usage can be nearly zero. Such MEMS dividers are expected to enable exceptionally low-power frequency synthesizers for applications where the operating frequency remains within the tuning range of the MEMS resonator, such as the Chip-Scale Atomic Clock (CSAC). Indeed, commercial CSACs presently consume a battery-unfriendly 120 mW

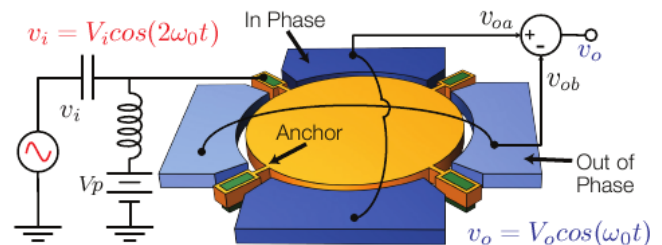


Fig. 2. Schematic of the differential frequency divider used on a single disk in order to boost divided output voltage swing and minimize common-mode harmonic feedthrough.

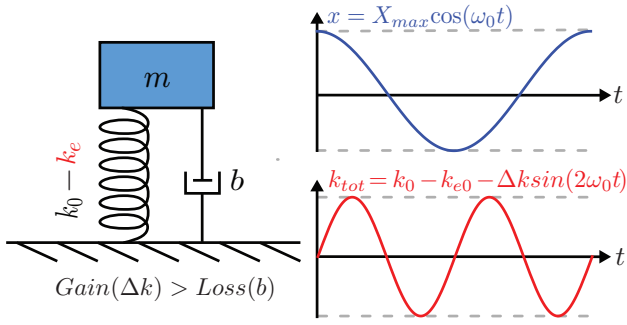


Fig. 3: Theoretical representation of the parametric oscillator divider consisting of a resonator (mass-spring-damper) undergoing motion at frequency ω_0 (blue curve). When stiffness, k , is modulated as in the red curve, restoring force is increased following x maxima and decreased near zero, leading to a parametric gain effect on motion.

[7], with a good portion of this burned by the frequency dividers in their synthesizers.

PARAMETRIC OSCILLATION

In a parametrically-driven device, an applied pump modulates a frequency-determining “parameter”, realized here as the electrical stiffness k_e , arising from the applied voltage across the electrode-disk capacitive gaps [6]. This gives rise to the equations of motion

$$m \frac{\partial^2 r}{\partial t^2} + \frac{m\omega_0}{Q} \frac{\partial r}{\partial t} + [k_0 - k_e(t)]r = F(t) \quad (1)$$

$$k_e(t) = \frac{1}{2} \frac{\partial^2 C_0}{\partial r^2} [V_g(t)]^2 \quad (2)$$

where m is effective resonator mass, r is effective radial resonator displacement at a location of maximum displacement amplitude, ω_0 is the resonance frequency, k_0 is the effective mechanical spring constant of the resonator, $F(t)$ is the resonator driving force (here, comprised of random thermal noise only), C_0 is the resonator-to-electrode capacitance, and V_g is the total voltage applied across this capacitive gap.

Driving V_g with an ac signal v_i at twice the resonance frequency, together with dc bias voltage V_P , generates electrical stiffness $k_e(t) = \Delta k \sin(2\omega_0 t) + k_{e0}$ composed of a static shift k_{e0} combined with a modulation component at twice the resonance frequency with $\Delta k \propto C_0 V_i V_P$. This modulation, illustrated in Fig. 3, leads to an increase in restoring force following max displacement and decrease near zero resulting in a phase-dependent parametric gain of resonant motion. For resonator motion at the correct phase relative to the parametric pump, this can be found [8] to give an amplitude gain of

$$G = \frac{1}{1 - Q\Delta k/2k_0} \approx \frac{1}{1 - \Delta f Q/f_0} \quad (3)$$

where Δf is the amplitude of frequency shift induced by the modulated stiffness. Though produced entirely by modulation of the resonator frequency, this gain can be understood conceptually as equivalent to a traditional oscillator where resonator motion is amplified in a closed-loop configuration. Recognizing f_0/Q as the 3 dB bandwidth of the resonator and, therefore, equivalent to the resonator damping, makes clear the equivalence of amplifier gain with depth of the applied stiffness modulation. When driven with sufficient pump

strength, this gain overcomes resonator losses and amplifies the, initially Brownian, motion into steady-state oscillation at the fundamental resonator frequency, limited only by resonator nonlinearities. Eqn. (3) in fact can be seen as the classic positive feedback equation with loop gain equal to the ratio of frequency pull over 3 dB bandwidth, $A_l = \Delta f/(f_0/Q)$.

Given the above mechanism for parametric gain, the use of such a device as a frequency divider is clear: an input electrical drive at twice resonance frequency atop a dc-bias voltage V_P produces a parametric gain via modulation of the electrical stiffness of the capacitive gap. When sufficient input voltage swing at $2f_0$ is provided, the parametric gain drives the resonator into oscillation at f_0 , the motion of which, when combined with the bias voltage, generates an output frequency-divided electrical signal.

As the parametric frequency modulation is produced by a time varying voltage applied across a pure capacitance, the power required for this drive can be, in principle, limited only by the energy transferred to the mechanical resonator. For a steady-state oscillator, this power transfer must be sufficient to balance resonator losses. With the extremely high Q achievable in MEMS resonators, this energy loss rate is tiny, requiring less 100 nW to sustain full oscillation amplitude for a typical Q of 90 k at 61 MHz.

DEVICE DESIGN AND OPERATION

To be useful in modern PLL applications, the MEMS resonators used must possess both high operating frequency and the capability to accurately define multiple unique frequencies on the same die, i.e., their frequencies should be definable via CAD layout. To this end, the wine-glass disk resonators depicted in Fig. 1(a) and Fig. 2 are quite suitable. These devices comprise 2 μm -thick, 32 μm -radius polysilicon disks supported by beams at quasi nodal points and coupled along their sidewalls to input-output electrodes by tiny 40 nm capacitive gaps. In the three-device array, coupling beams sized to correspond to half the acoustic wavelength force the individual resonators to move in-phase at a single resonance, allowing output current to add constructively to boost electromechanical coupling by the number of individual resonators [9]. To excite the composite resonator into motion, a bias voltage V_P on the disk structure combines with an ac drive voltage applied to all input electrodes to produce forces across the input electrode-to-resonator gaps that, at resonance, excite the wine-glass (i.e., compound (2, 1)) mode shape, shown in the inset of Fig. 1(b). The frequency of resonance is given by [10]:

$$f_{nom} = \frac{K}{R} \sqrt{\frac{E}{\rho(2+2\sigma)}} \left[1 - \frac{k_e}{k_0}\right]^{\frac{1}{2}} \quad (4)$$

where R is the disk radius, $K = 0.373$ for polysilicon structural material, k_e is the electrical stiffness given by Eqn. (3), and E , σ , and ρ are the Young’s modulus, Poisson ratio, and density of the structural material, respectively.

To exploit the parametric amplification effect for frequency division, the lateral 40 nm capacitive gap of the device of Fig. 1(a) produces both the strong voltage-dependent frequency tuning, cf. Fig. 1(c), required for parametric excitation and, with a bias voltage, an output current propor-

	Q	Radius [μm]	Gap [nm]	h [μm]	m [ng]	k_0 [N/m]	C_0 [fF]	f_0 [MHz]	V_P [V]	v_i [mVpp]	v_o [mVpp]
Array Device	91 k	32	40	2	16.1	23.0×10^5	106.8	60.587	4	700	265
Differential Device	84 k	32	40	2	5.37	5.37×10^5	35.6	60.560	4	445	450

Table 1. Design and measured values for the fabricated MEMS dividers

tional to the resonator motion. By enhancing tuning, the small capacitive gaps enable parametric oscillation at UHF frequencies well beyond the kHz range of earlier parametrically amplified sensors [11], and further allow adjustment of the operating frequency of the divider, as needed for many real-world applications.

NOISE FILTERING

Because the MEMS resonator used here has such high mechanical Q , it responds with long time constants to changes in the input signal, and so effectively filters out noise signals not within its bandwidth. This means that when operated as a self-sustained parametric oscillator, this device removes oscillation perturbations at frequencies greater than the bandwidth of the resonator. Though similar in principle to injection-locked oscillators or PLLs where far-from-carrier phase noise is suppressed, the extremely high Q -factor of the MEMS resonator deployed here produces a pronounced filter cut-off even at frequency offsets below 1 kHz. Combined with the lack of active devices, hence lack of associated noise, the MEMS-based parametric oscillator provides not only divide-by-two frequency division with the expected 6 dB phase noise reduction, but also additional filtering of phase noise outside of the resonator bandwidth. It should be noted that while an effective narrow lock range of the oscillator provides additional filtering, the operating frequency can still be tuned over a much larger range through use of the voltage-controllable electrical stiffness, allowing this device to operate over appreciable bandwidths.

EXPERIMENTAL RESULTS

Using Eqn. (4), the single-disk differential device and 3-disk single-ended array device summarized in Table 1 were designed to provide divide-by-two functions with 120-MHz input and 60-MHz output. The fabrication process used for the devices was based on a surface micromachining process similar to that of [5], summarized in the cross sections of Fig. 4. The devices and electrical interconnect were fabricated from polysilicon deposited via Low-Pressure Chemical-Vapor Deposition (LPCVD) at 615°C, in-situ doped with phosphorus. A High-Temperature Oxide (HTO) deposition provided the high-quality sacrificial sidewall spacer that enabled 40nm electrode-to-resonator gaps. Two Chemical-Mechanical Polishing (CMP) steps, one before structural polysilicon deposition and patterning and the other after the electrode polysilicon deposition, provided the planar surfaces needed for precise lithography, as well as removed electrode-disk overhangs that can cause pull-in and device failure at low bias voltages. Fig. 5 presents SEMs of fabricated devices along with FEM simulations of their mode shapes.

Devices were tested in a Lakeshore model FWPX vacuum probe station capable of providing 10 μTorr vacuum.

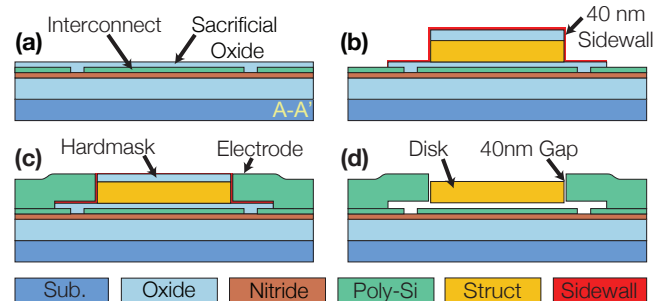


Fig. 4: Fabrication process consisting of repeated thin-film polysilicon and oxide deposition and etching on a silicon substrate, achieving, first, the electrical interconnect of (a). Subsequent depositions and etching yields the structure and thin oxide sidewall sacrificial of (b), after which a polysilicon deposition, patterning and CMP gives the planarized structure of (c). Finally, a wet-etch in 49% HF yields the released resonator structure of (d).

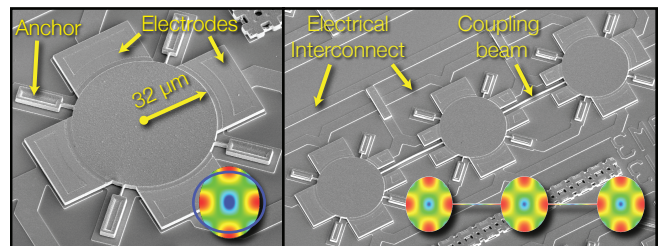


Fig. 5: SEMs of the released frequency-dividers measured in this work with (left) a single-disk, differential and (right) a 3-disk arrayed single-ended divider. Inset FEM simulations illustrate the resonance mode shapes.

A GGB Industries Picoprobe model 35, modified to operate in the Lakeshore vacuum system, provided accurate divider input and output voltage measurement with minimal signal loading. Phase noise was measured on an Agilent E5505A phase noise measurement system.

Fig. 6 presents the output of an arrayed device like that shown in Fig. 1(a), driven by 700 mVpp at 121.174 MHz. The resultant 60.587-MHz oscillation combined with a 4 V bias voltage generates a current at the output electrode that drives the modestly large 350 fF output capacitance (composed of bondpad plus Picoprobe capacitance) to a 265 mVpp swing. While the output-to-input voltage ratio is below unity in this configuration due to the large output capacitance, the generated output current would be sufficient to produce an output voltage swing equivalent to input when driving the much smaller 50 fF capacitance of an integrated 2nd MEMS division stage or on-chip buffer.

To achieve an output voltage of similar magnitude as the input even in the face of large bondpad capacitors, the balanced wine-glass disk configuration of Fig. 2 using a differential output was also investigated. Here, driving the pump

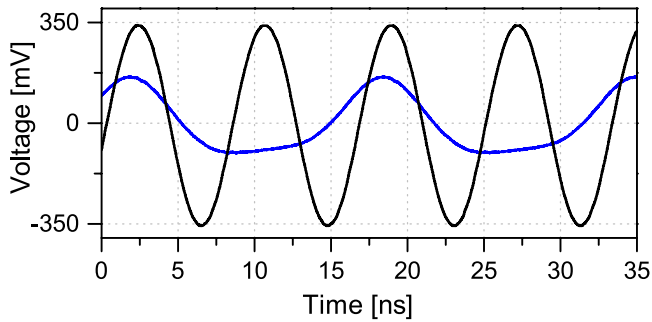


Fig. 6: Input 121.2-MHz pump (black) and resultant 60.6-MHz output waveform measured on the single-ended divider. Input and output signals spanned 700 mVpp and 265 mVpp, respectively. Distortion can be seen in the output waveform due to feedthrough of the pump signal.

signal on the disk itself not only enhances the electrical stiffness, which now derives from all electrodes, but also doubles the differential output swing, all while canceling common-mode feedthrough. The resultant output swing shown in Fig. 7 spans 450 mVpp using only a 445 mVpp pump. Thus, voltage gain is provided, as needed for a cascaded divider chain, without need for power-hungry active devices.

Fig. 8 presents measured phase noise of the single-ended divider output when driven by a custom-built VCO with mediocre phase noise, showing the 6 dB improvement for close-to-carrier phase noise expected due to frequency division. Perhaps more impressively, the high- Q resonator response provides filtering of noise past a 1 kHz offset, leading to a remarkable 23 dB decrease in far-from-carrier phase noise, limited only by the poor 50 nV/rtHz noise performance of the Picoprobe used to measure the output.

CONCLUSIONS

Through use of a parametric amplification effect enabled by the electrical stiffness of capacitive gap MEMS resonators, a new type of frequency divider has been demonstrated. This divider provides both the expected 6 dB phase noise improvement close to carrier for a divide-by-two function as well as additional noise filtering for offsets above 1 kHz due to the high- Q mechanical response function—a unique advantage of this MEMS technology. Consuming only 100 $\mu\text{m} \times 100 \mu\text{m}$ die space for a single 120-MHz divider, this MEMS-based approach further offers significant space savings over similar CMOS based dividers [12], where bulky inductors consume 750 $\mu\text{m} \times 320 \mu\text{m}$ for an operating frequency of 20 GHz, and offer no possibility of division down to typical reference frequencies, e.g., 10 MHz. Adding to the list of benefits, as frequencies increase, this MEMS-based frequency divider shrinks in size: A 3.4-GHz version would occupy under 30 $\mu\text{m} \times 30 \mu\text{m}$ of die area. Future efforts to design frequency-matched chains of such MEMS dividers would be expected to enable complete low-power PLL topologies at up to GHz frequencies. Clearly, this device adds a previously missing frequency divider capability to the MEMS toolbox.

Acknowledgement: This work was supported under the DARPA CSSA program.

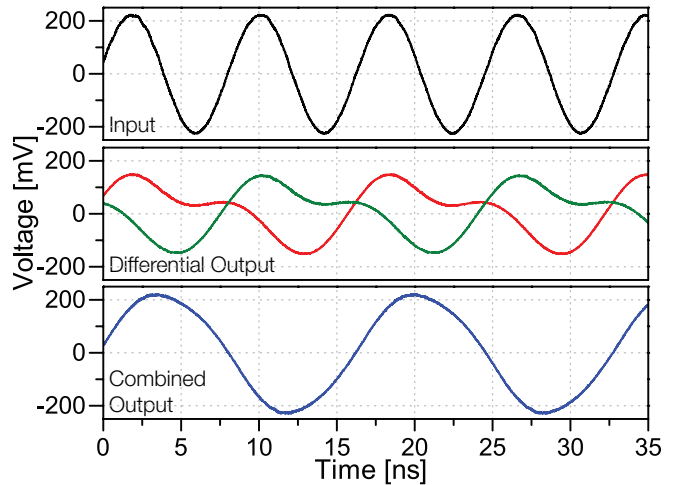


Fig. 7: Single-disk differential measurement with a 445mVpp input pump (top), separate differential outputs (middle) and combined differential output of 450mVpp (bottom).

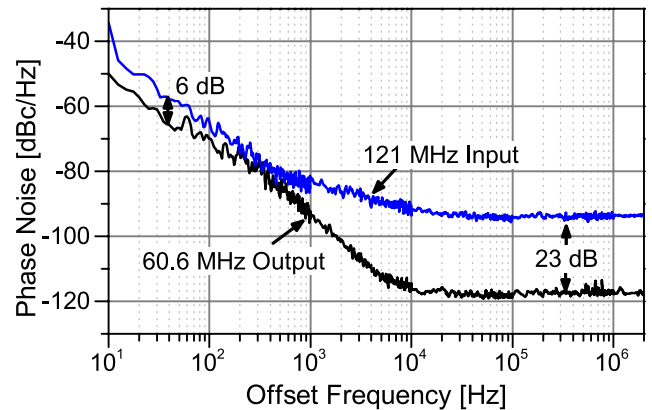


Fig. 8: Single side-band phase noise comparison of input pump signal from a low quality VCO operating at 121 MHz and resultant 60.6-MHz output of the single-ended divider. Phase noise shows both the expected 6 dB improvement, but also additional filtering from the high Q of the resonator.

REFERENCES

- [1] ON Semiconductor, Divide by 16 Divider, Part: NB6N239S
- [2] M. Tiebout, *JSSC*, vol. 39, pp. 1170-1174, 2004.
- [3] P. Dubey and R. Agarwal, *Proceedings, VLSI Design*, 2013, pp. 158-162.
- [4] S. Verma, *et al.*, *JSSC*, vol. 38, pp. 1015-1027, 2003.
- [5] M. A. Abdelmoneum, *et al.*, *Proceedings, IEEE Int. Conf. on MEMS*, 2003, pp. 698-701.
- [6] H. C. Nathanson, *et al.*, *IEEE Transactions on Electron Devices*, vol. 14, pp. 117-133, 1967.
- [7] Symmetricom CSAC model number SA.45
- [8] D. Rugar and P. Grütter, *PRL*, vol. 67, p. 699, 1991.
- [9] M. U. Demirci and C.-C. Nguyen, *JMEMS*, vol. 15, pp. 1419-1436, 2006.
- [10] M. Onoe, *JASA*, vol. 28, p. 1158, 1956.
- [11] M. J. Thompson and D. A. Horsley, *J-MEMS*, vol. 20, pp. 702-710, 2011.
- [12] W. Lee and E. Afshari, *JSSC*, vol. 45, pp. 1834-1844, 2010.

Contact: Tristan O. Rocheleau, Tel: +001-607-232-2162; tristan@eecs.berkeley.edu